

## DEVELOPMENTS AND APPLICATIONS OF HIGH POWER AND HIGH REPETITION LASERS; FROM THE LASER FUSION TO THE INDUSTRIAL NEUTRON SOURCES

**Kunioki Mima<sup>1</sup> and Koichi Kasuya<sup>2</sup>**

1) Graduate School for the Creation of New Photonics Industries, Hamamatsu, Japan

[k.mima@gpi.ac.jp](mailto:k.mima@gpi.ac.jp)

2) Institute of Applied Flow, Yokohama, Japan and Institute of Laser Technology, Osaka, Japan

[kasuya.koichi@ilt.or.jp](mailto:kasuya.koichi@ilt.or.jp)

The present status of laser fusion researches in Japan is described. In the first, the fast ignition laser fusion is the high-light of high power laser applications. The recent progress of fast ignition research project at Osaka University: FIREX will be reported.

As the industrial applications of laser produced neutron and X-ray, it is explored how they are used for diagnosing the chemical and physical processes in fuel cell and other chemical energy converters. These applications are also important topics of this talk.

As the laser fusion reactor technology, we will also present “UV Laser Ablations and Erosions to Investigate Fusion Reactor Surface Material Interactions, Hydrogen Storage Thin Layers Formations and the Related Subjects”.

### 1. Introduction

Laser fusion is a unique scheme in comparison with the other fusion schemes like Tokamak and Helical devices. In laser fusion, a tiny pellet is irradiated with many high power laser beams to compress the fusion fuel to 1000 times solid density which is higher than the plasma density at the center of the sun and the part of the compressed fuel is heated up to 10 keV to be ignited. As shown in the Fig.1, several times every one second, a fusion fuel pellet is injected into the reactor chamber to generate fusion energy of a few giga watt and about one giga watt electric power will be sent out to the grid. The key issues which should be investigated are the ignition and burn of the compressed fuel at present, and the high average power high efficiency laser technology, high repetition rate reaction chamber design, and continuous pellet injection in future.

There are two main schemes for pellet implosion, i.e., direct and indirect drive[1]. In the direct-drive implosion, the surface of a fuel pellet is irradiated directly by laser beams. In contrast, in 'indirect-drive implosion', the driver energy is converted into soft x-rays, which fill a cavity. The soft x-rays are then absorbed on the surface of the pellet to generate ablation pressure to drive the implosion. As the indirect fusion drivers, laser beams, Z-pinch with pulse power or heavy ion beams have been widely investigated. In the case of heavy ion beams, they deposit the energy in radiation-emitter foils placed at symmetry positions inner the beam entrance holes of hohlraum. Then emitted radiations are confined in the hohlraum and implode a fuel capsule.

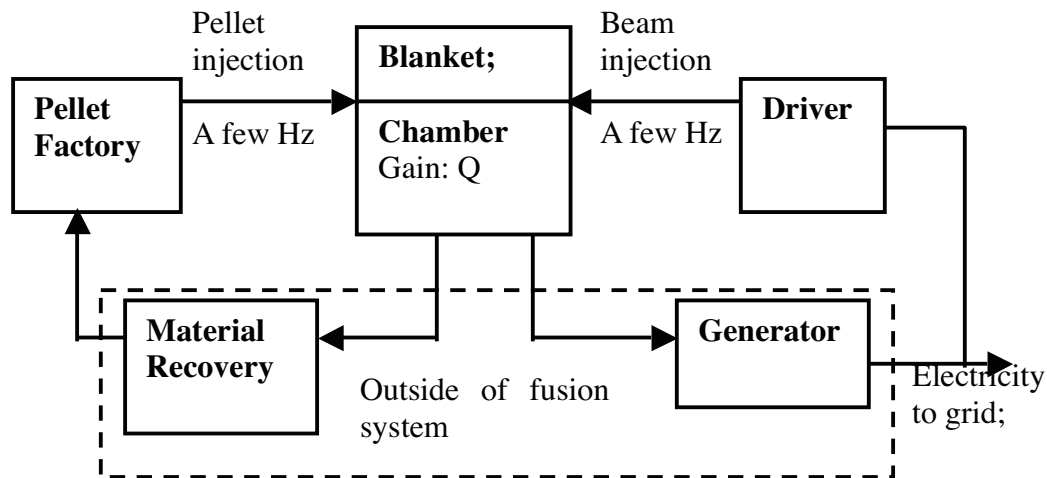


Figure 1 Energy and material flow diagram in laser fusion power reactor

The direct implosion and the indirect implosion have merits and demerits. The merit of the direct implosion is the high coupling efficiency from input laser energy to the imploded core plasma energy. The demerit is the implosion hydrodynamic instability and spherical uniformity. So, much higher laser irradiation uniformity is required for direct drive. On the other hand, the merit of the indirect drive is the high implosion uniformity and the stability because of the X-ray drive. However, the demerit is the low implosion efficiency. So, larger laser energy is necessary for ignition and high gain.

The ignition and burning in the indirect implosion will be demonstrated in a year or so. On the other hand, the feasibility of the direct drive ignition was demonstrated by the high density compression experiments at the Institute of Laser Engineering(ILE), Osaka University [2] , and the Laboratory for Laser Energetics, University of Rochester [3]. In the ILE experiments, targets made by DTCH plastic were imploded with Gekko XII laser smoothed by Random Phase Plate (RPP) invented at ILE, Osaka [4] to compress pellets to 600g/cc. In the Rochester experiments, deuterium filled targets are imploded to 100 times solid density. Recently, the up-grade OMRGA experiments demonstrated 500 time compression of a D<sub>2</sub> cryogenic target .

The present prediction of fusion gain and ignition for the indirect drive and the direct drive indicates that the laser energy for the indirect drive ignition is estimated to be about 1.8MJ and that for the direct drive ignition will be less than 1 MJ. After the ignition demonstration for the indirect drive in NIF, NIF will be devoted to direct drive and fast ignition demonstration.

Since new laser technology so called Chirped Pulse Amplification (CPA) was invented by D. Strickland and G. Mourou [5], ultra intense short pulse laser technology advanced rapidly. Actually, the peak power of short pulse laser has been increasing by factor 2 annually after it reached over 1TW in 1990. The peta watt ( 10<sup>15</sup> W) lasers were constructed in 1998 at LLNL and in 2001 – 2004 at ILE, Osaka University, and at Rutherford Appleton Laboratory. The ultra-intense laser technology development introduced the new fusion concept so called “fast ignition”. It was proposed by T.Yamanaka [6], N.Basov [7], and M.Tabak [8]. In the radius of the hot spark where the ignition starts is much smaller than that of the central ignition hot spark, since the density, so, the pressure of

fast ignition hot spark is much higher. Because of this, the laser energy required for the fast ignition could be smaller than that for the central ignition by one order of magnitude as shown. Furthermore, in the isobaric implosion core for high gain, the hot spark radius is about half of the total radius. Therefore the plasma  $\rho R$  for fast ignition could be 2 times larger than that for the central ignition when the implosion laser energy is the same. This is the reason why the fusion gain is higher for the fast ignition. This is the most important merit of the fast ignition. The demerit of the fast ignition is that novel laser technology is required and that the heating physics is not matured. However, very many research programs are progressing or planned to solve the problems. The FIREX-I project at ILE, Osaka University, and OMEGA-EP project at LLE, University of Rochester are examples. They are important projects for demonstrating the efficient heating of imploded plasmas to produce ignition equivalent density and temperature plasmas. The LFEX laser for FIREX-I and OMEGA-EP laser which started operation recently,

## II. FIREX PROJECT at Osaka University

By the PW laser experiments, the imploded plasma has been heated up to about 1 keV.[9] in the Joint experiments of Osaka University and Rutherford Appleton Laboratory to clarify the heating scaling law in the relations between heating laser energy, hot spark temperature and neutron yield. Using the Fokker-Planck simulations, cone shell target experiments were analyzed. Relativistic electrons are generated more efficiently and the spectrum is predicted to be double Maxwellian. Then, the ion temperature will reach higher than 1keV . The results can be extended to the FIREX. Namely, the coupling efficiency is higher than 10% and the required heating laser energy for achieving 5keV (The goal of Fast Ignition realization Experiment I; FIREX-I) is estimated to be 10kJ for 100 times solid density DT plasmas with 30  $\mu\text{m}$  diameter.[2] For the fast ignition, the critical parameters are the hot spot radius,  $r_b$  and the coupling efficiency which strongly depend upon the relativistic electron spectrum, source stand-off distance, and transport. According to the simulation and precious experiment results, the relativistic electron heat flow can be confined by self-generated magnetic fields in the cone shell target. Then, the deposited laser energy is concentrated at the top of the cone and the hot spark radius could be controlled by the cone tip radius and the position of the cone tip. From the present understanding on the heating processes, the ignition can be achieved with a pulse energy less than 50kJ / 10psec for an imploded plasma  $\rho R$  higher than 1.0 g/cm<sup>2</sup>.[10] ,[11]



Figure 2 10kJ/ 10ps LFEX laser

For demonstrating the feasibility of the fast ignition, the LFEX laser have been completed at Osaka university (Laser for Fast ignition Experiment: LFEX) : FIG.2. The LFEX is coupled with the Gekko XII laser of 10kJ/ ns with 0.53  $\mu\text{m}$ . The one beam experiment with the LFEX has started. However the preliminary experiments indicate that the enhancement of neutron yield is not high as it was expected because of the laser pre-pulse. So, toward the FIREX-I , an advanced target is proposed for achieving better heating performance. The designed target is shown in the Fig.3. Here, we introduced the thin foil on the laser entrance of the cone, the double cone wall, low Z (Plastic) coating of the inner and the outer surfaces which leads to higher implosion  $\rho R$  (as indicated by Nagatomo [12]) , and the Br doped ablator of the fuel shell for stabilizing the R-T instability.

In this paper, we will summarize the results of the preliminary experiments and discuss about the physics related to the advanced target.

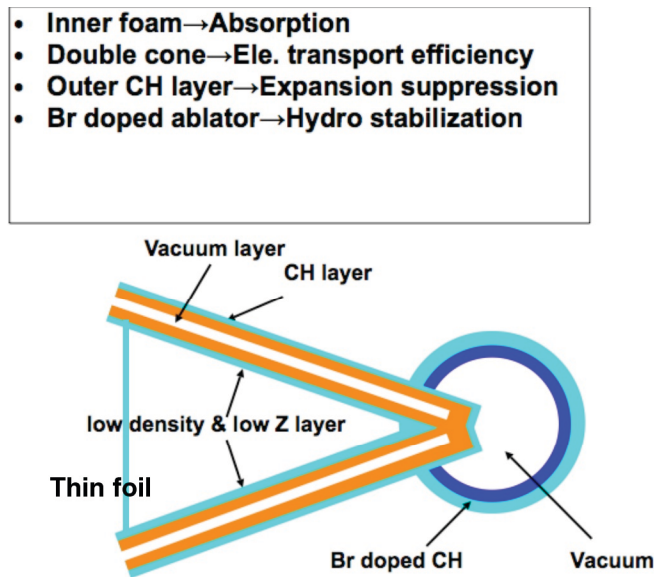


Figure 3 Advanced target design for FIREX-I [11][13]

## 2. Summary of the preliminary results of the FIREX-I experiments

The 10kJ/ ps short pulse laser LFEX, for fast ignition, was dedicated on March 2009. The heating experiments started in June of 2009. The one beam of the heating laser was injected into the cone. The shot timing is measured by the X-ray streak camera. The results indicate that LFEX X-ray signal and X-ray from the imploded core are coincident. Namely, a peta watt laser pulse could be synchronized with the maximum compression timing. In this case, the neutron yield is enhanced. The plasma profile inside the cone is also measured by the X-ray image. The Fig.3 shows the time integrated x-ray image together with neutron yield. The X-ray image of Fig.3(a) indicates that the LFEX beam is focused at the center of the cone but absorbed at 100~200  $\mu\text{m}$  away from the cone tip. The neutron yield increased by a factor of 30 from that without heating. Ion temperatures are

deduced from the neutron yield, fuel density and the fuel mass as shown in Fig.3(b). We found that the ion temperature strongly depend upon the laser pulse width. When the pulse width is shorter than 2 ps, the neutron yield and the ion temperature are higher. From the above experimental results, long scale pre-plasmas are produced inside the cone and the main laser pulse is absorbed 100~200  $\mu\text{m}$  away from the cone tip. we presume that the LFEX laser pre-pulse produces plasmas. Because of the long scale pre-plasma by Kemp etal [14], significant amount of hot electrons with energy higher than 10MeV are generated in the under dense plasmas. These pre-pulse effects result in decoupling between the hot electrons and the compressed core. So, the enhancement of the neutron yield is 30 times in comparison with the no heating case and much smaller than the previous case. [Kodama etal, Nature][9]

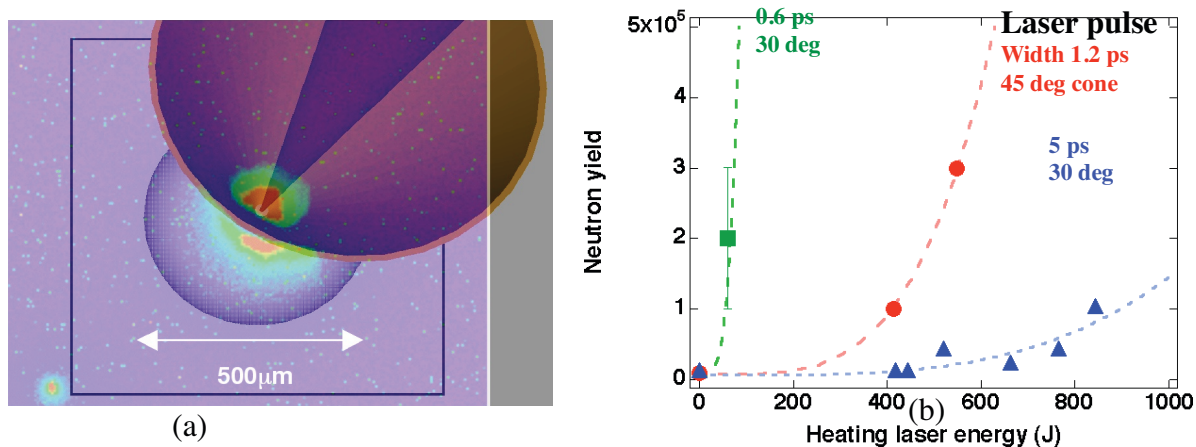


Figure 4 (a) X-ray pinhole image of the plasma inside the cone and the imploded plasma, (b) neutron yields for the 2001 experiment, FIREX experiments with 5 psec and 2 psec heating pulse.

In summary, the multi beam LFEX laser will be completed by the April 2010 and the full beam LFEX experiment will start in 2011. The imploded dense plasma is expected to be heated up to the ignition temperature in 2011. In the experiments of the 2010 fall, the advanced target shown in the Fig.3 will be used. The heating laser will be the two beam of the LFEX and the 2kJ pico second laser energy will be injected. The ion temperature will reach 2keV. This is the important milestone toward realizing the 5keV ignition temperature.

### III. Generation of neutrons, particle beams by high power laser and applications

Neutron generation by short pulse laser of order of ns to fs have been well investigated for many years. The physical model of typical examples is shown in Fig. 1. They are ①gas cluster target, ② thin film target, ③spherical pellet target for implosion. There are many optimized structures of each target such as density control, composite material and Z number optimization, layered structure etc. The pulse width and shape are also optimized according to the type of the targets and structures, of which features are also shown in Fig. 5.



### Generation of Neutron and Beams by High Power laser

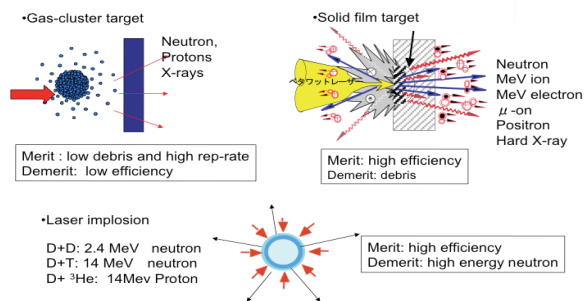


Fig. 5

### Neutron Yield Scaling with respect to Laser Energy

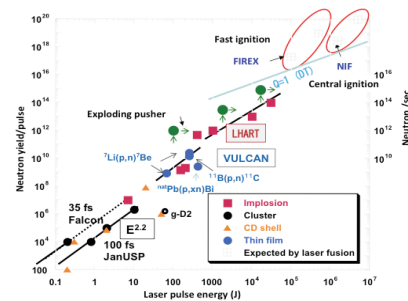


Fig. 6

Fig. 6 shows the compiled data of neutron generation as a function of injected laser energy with different pulse width depending on the related physical processes. The data points are basically single shot results. The rep-rate operation is needed for the industrial application as a neutron source. For this purpose, repeatable target feeding and high average power pulse laser must be developed. The right vertical axis shows the neutron fluence per second when the neutron production shots are repeated at 10 Hz to 1 kHz. It should be noted that fusion ignition can enhance the neutron production beyond the line  $Q=1$  where the fusion energy is equal to the incident laser energy, and also it is expected to be demonstrated in near future of 2010~2015.

### III. 1 Industrial Applications of Laser Neutron Source

The applications of neutron sources in science and industry are discussed in the previous report in IFSA2007[15]. It spans over wide fields of material science and technology, nuclear energetics, medical, and new methodology in diagnostics, especially in measurements of light elements such as Hydrogen and Li.

The required source neutron flux is evaluated from the necessary neutron energy and flux density at the sample of the specific application, and the design of energy moderation and guiding of neutrons. For the diagnostics of Li-ion battery and fuel cell, thermal neutron flux of  $10^{11} \sim 10^{12}$  /sec is required. For the medical applications like BNCT, the flux is  $10^{12} \sim 10^{13}$  /sec. For semiconductor doping (NTD), the flux is  $10^{13} \sim 10^{14}$  /sec. For material processing like annihilation of radio-activity in which long life radio-active elements in a used nuclear fuel are transmuted by fusion neutron, fusion material test, and fusion- fission hybrid in which a under critical fission reactor is driven by fusion neutron irradiation, the flux higher than  $10^{15}$  /sec is required.

In the following section, the laser driven nuclear processes are discussed for the applications to the new diagnostics which are necessary for the developments of Li ion battery and Hydrogen fuel system.

### III.2 Application of Laser Produced Neutron and Ion to Li-ion Battery Diagnostics

In the R&D of the lithium ion battery, it is necessary to diagnose the damage of electrode and the dynamics of lithium and negative ions in the electrodes and electrolyte. Neutrons and ions are appropriate and unique tools for the Li-ion battery diagnostics. However, because the conventional

irradiation facilities are huge and nowadays only specialized nuclear research site can be used, the speed of material developments for the advanced battery is limited. Neutron and ion sources driven by lasers could provide a compact combined system for this purpose. The applications of laser driven neutron and ion for observing electrodes, lithium, negative ions are discussed here. The images of diagnostic systems are the facility at University of Texas in the reference[16] for neutron diagnostics and the Fig. 7 for proton diagnostics. Here, an intense short pulse laser irradiates a solid target or cluster to generate mono-energy protons. Laser produced MeV protons are guided and directly injected onto the Li-ion battery to probe Li-ion depth profile, negative ion depth profile and so on. Otherwise, the protons are injected into liquid Li metal target to generate low energy neutrons. The neutrons are decelerated to thermal neutrons that are used for the Li battery diagnostics as discussed in the reference [17] or in some other new methods.

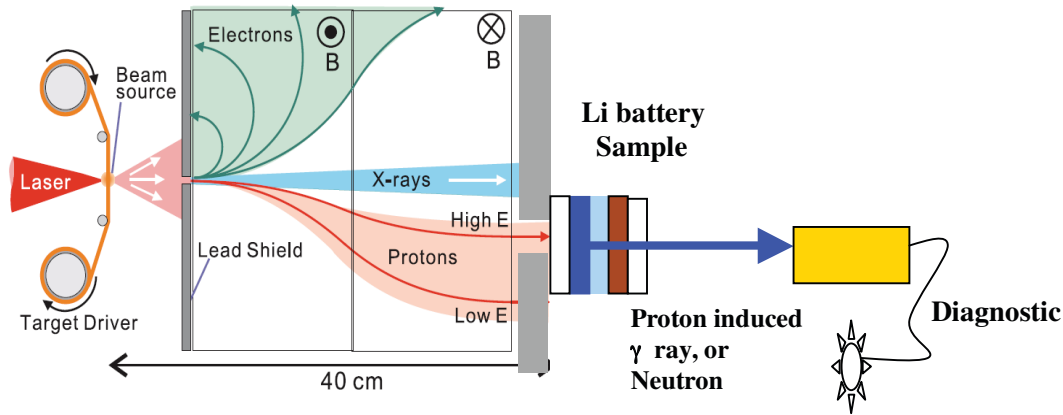


Figure 7 A schematic diagram of application of laser produced proton beam to

On the other hand, neutrons generated by ultra intense short pulse laser can be also applied for the Li battery diagnostics. The thermal neutron scattering, excitation, and reactions of light elements are used for the diagnostics. As an interesting example, we describe the application of neutron absorption reaction. The reaction:  ${}^6\text{Li} + n \rightarrow t(2.7\text{MeV}) + \alpha(2.1\text{MeV})$  could be used for measuring Li depth profile by observing the emitted T and/or  $\alpha$  energy spectrum. Namely, the T and  $\alpha$  energy spectra correspond to the Li number density. The lowering of energy of T or  $\alpha$  corresponds to depth of the place where the reaction takes place. In this way, the Li depth profile can be measured[18] Multi-MeV protons generated by laser are used for generating sub-MeV neutrons through p-Li reactions.

### III.3 Laser produced proton diagnostics

When MeV protons are injected into Li- battery, protons react with light nuclei like Li, F, and so on to produce  $\gamma$  rays and/or neutrons. Since these nuclear processes are threshold reaction, we can deduct ion density depth profile from the proton beam energy dependence of  $\gamma$  ray yield and/or neutron spectrum. The proton induced  $\gamma$  ray diagnostics has been known as the PIGE (Proton Induced Gamma Emission)[18]. Energy spectrum of neutrons induced by the reaction  ${}^7\text{Li}(p, n){}^7\text{Be}$  can be used for diagnostics of Li depth profile, since neutron energy depends on proton energy.

Although the energy spread is the critical issue, the laser produced protons are unique as a probe beam because of very low transverse emittance and short pulse. The energy spread could be overcome by introducing energy selector as shown in *Figure 7*. Let's take a quasi mono-energy proton beam with  $(\Delta E / E)_{\text{FWHM}} \sim 0.1$ [19]. For obtaining a beam of 1% energy spread, 10% of the total flux can be used. In the case of Li ion battery, the width of a typical sample is 200  $\mu\text{m}$ . Therefore, the spatial resolution obtained by this proton beam diagnostics like PIGE could be a few  $\mu\text{m}$ . This resolution is not very good, but interested in the field of Li ion battery community.

#### **IV. Application of laser displacement sensor to monitor inner surface condition of nuclear fusion reactor chamber**

For many years we investigated the erosion of the candidate of fusion plasma facing wall materials with intense pulsed ion, electron, laser and x-ray beams. One of the most useful diagnostic methods in our experiment was a laser surface profiler to measure the exact profile of the eroded surface. After our pileup of such data, we came to propose a new application of such profilers to inner surface condition monitors for nuclear fusion reactor chambers. During the successive nuclear fusion burn, it is very important to observe the inner surface condition of the chamber for the purpose not to destroy the chamber, or to predict the dangerous hazard to the chamber in advance. We hope that our new proposal becomes one of the methods to solve such crucial problems. As we have the maximum page limit of this article, below are shown the most recent fundamental data of the erosion measurements, in short. The more details of erosion investigations and the preliminary monitor system with commercial surface profilers are described in an accompanied article in this meeting [IV-1]. Such monitor system is useful both for magnetic and inertial fusion energy.

##### **IV.1 Surface profiler with laser displacement sensor**

We used a commercial laser displacement sensor (Keyence / Model LE-4000) with a Coms/MAP-2EM-50X sample-stage precise control. Samples were placed on a small X-Y table, which was moved with two precision motors under the computer control. A red semiconductor laser placed above the table was injected on to the sample surfaces, and the reflected and/or scattered laser light was observed with a CCD detector. With these arrangements, the three dimensional surface profiles were obtained for various sample surfaces. A software program installed in a desktop and/or laptop computer were used to get and make analyses of the sample surface profiles.

##### **IV.2 Electron beam thermal erosion associated with ELM-divertor simulation**

We used a JEBIS apparatus in JAEA Naka Laboratory and produced pulsed electron beams (of about 1ms time duration and  $1\text{MJ}/\text{m}^2$  fluencies) to irradiate various samples. The equivalent thermal erosion might be able to simulate the divertor-ELM (edge localized mode) state. Under the electron acceleration voltage and current of 65kV and 2.28A, and under the three kinds of beam pulse width, the thermal loads on the sample surfaces were a) 1.0ms:  $1.10\sim 1.20\text{ GW}/\text{m}^2$ , b) 1.2ms:  $1.40\sim 1.45\text{ GW}/\text{m}^2$  and c) 1.5ms:  $1.46\text{ GW}/\text{m}^2$ .



We tried to make an active estimation of the equivalent threshold thermal load for tungsten surface erosion, and the comparison with the carbon case value, reported. The craters produced with the electron beams are shown in *Fig.8*. This is the case with a single shot on the surface of about 10x10 mm<sup>2</sup> size, and both of the beam conditions and a scale are shown in the same figure. With the increase of the pulse width, we observed the increase of two dimensional crater sizes. With the use of surface profiler described in the above section, we measured the crater depth as a function of pulse width. The result is shown in *Fig.9* With the numerical fitting line in the same figure (with the extrapolation down to the x-axis), we estimated the threshold pulse width to start the erosion, which, in turn, we obtained the threshold thermal load, as follows.

The simple estimation equation for the threshold thermal load on carbon divertor surface with ELM is shown in reference [21], as follows.

$$Q/ \Delta t^{1/2} = 45 \text{ MJ/m}^2/\text{s}^{1/2}, \quad (1)$$

where Q is the ELM thermal energy flux [MJ/m<sup>2</sup>] on the divertor surface, and  $\Delta t$  is the heat pulse width [s]. This equation is very shortly described in the same reference, there seems that there are no precise derivations (both theoretically and experimentally) there and also in other corresponding references. So that, we tried to tell the exact thermal threshold value in the tungsten case result shown in *Fig.9*. The pulse width of the fitting line cross point with the x-axis is about  $0.73 \times 10^{-3}$  [s]. We calculated the corresponding Q and  $\Delta t^{1/2}$ , and we finally got

$$Q/ \Delta t^{1/2} = 270 \text{ MJ/m}^2/\text{s}^{1/2}. \quad (2)$$

Here Q was about 1.0 [MJ] with the JEBIS calorimeter measurement (representative value). With the comparison of both equations (1) and (2), our sample tungsten was stronger than carbon by about  $270/45=6$  with roughly saying.

### IV.3. ArF laser erosion of tungsten measured with the same method

In our past experiment, ArF laser lights were focused on several samples to observe the surface erosion with the wavelength of 190nm. The nominal laser energy, the pulse duration, the spot size, and the laser fluencies in the past experiments were 600 mJ, 10 ns,  $0.7 \times 1.7 \text{ mm}^2$ , and 10-50 J/cm<sup>2</sup>. The same kinds of UV laser irradiations were revisited here again. Same kinds of sample irradiations with rather low energy laser lights with multiple laser overlapping up to 16,000 shots on the same spot were performed. The vacuum pressure of the sample chamber was between 2 and  $3 \times 10^{-1}$  torr. The repetition rate of the ArF laser was 5Hz. Tungsten, graphite and carbon were the materials here. The details about these experiments are described in [20]. One of the interesting subjects was again the erosion threshold measurement as was described in the above section of the electron beam erosion, The laser energy per shot changed between 357 and 230mJ.

The crater depth vs the total shot number of irradiations accumulated on the same surface spot is shown in *Fig.10* for the case of tungsten. The upper is the case with higher normal incident laser energy, while the lower is the case with lower normal incident laser energy. With the data line fittings, we obtained the both erosion thresholds as the crossing points of the x-axis (values, extrapolated). The erosion thresholds (the total shot number per spot) here were about 6 and 30 shots.

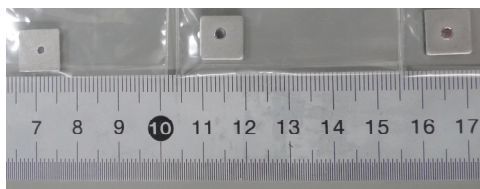


Fig 8 Tungsten erosion with pulsed electron beams.

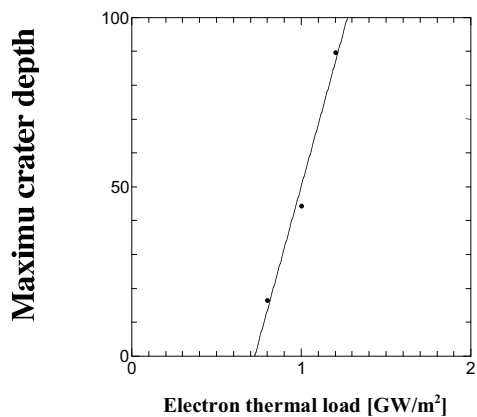


Fig.9. Maximum crater depth vs electron thermal load

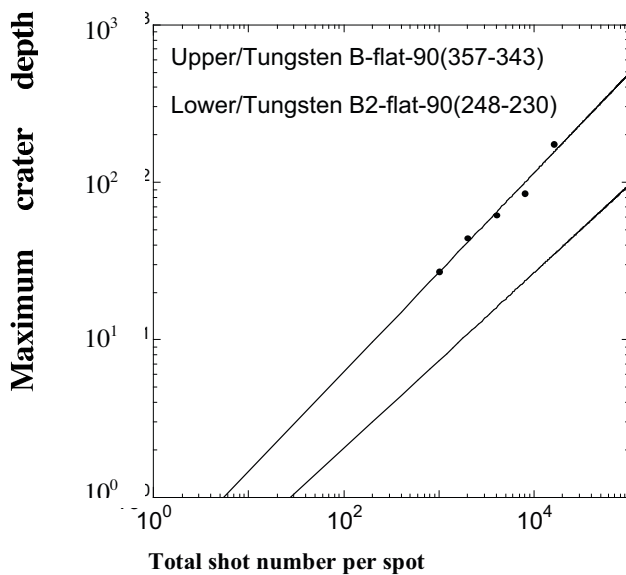


Fig.10 Maximum crater depth vs total shot number per spot

## Reference

- [1] Mima, K. Nuclear Fusion 50(2010)014006
- [2] Azechi, H et al, Laser and Particle Beams, vol.9, 193 (1991)
- [3] McCrory, R.L., et al, Plasma Physics and Controlled Nuclear Fusion Research, vol.3,17(1988)
- [4] Kato, Y., Mima, K., et al, Phys. Rev. Lett. 53, 1057 (1984)
- [5] Strickland, D. and Mourou, G., Opt. Communication. 56, 219(1985)
- [6] Yamanaka, T., Internal report of ILE, Osaka University, (1986)
- [7] Basov, N.G., Gus'kov, S.Yu., and Feokistov, L.P., "Thermonuclear gain of ICF targets with direct heating of ignitor", J. Soviet Laser Research 13 (1992) 396.
- [8] Tabak, M., Hammer, J., Glinsky, M.E., Kruer, W.L., Wilks, S.C., Woodworth, J., Campbell, E.M., Perry, M.D., and Mason, R.J., "Ignition and high gain with ultrapowerful lasers", Phys. Plasmas 1 (1994) 1626.
- [9] Kodama, R., Norreys, P.A., Mima, K. et al., Nature 412 (2001) 798, "Fast heating of super solid density matter as a step toward laser fusion ignition",.
- [10] Mima, K; Tanaka, KA; Kodama, R; Johzaki, T; Nagatomo, H; Shiraga, H; Miyanaga, N; Murakami, M; Azechi, H; Nakai, M; Norimatsu, T; Nagai, K; Taguchi, T; Sakagami, H, "Recent results and future prospects of laser fusion research at ILE, Osaka, EUROPEAN PHYSICAL JOURNAL D", 2007, 44, 259 ~ 264
- [11] H. Azechi, K.Mima, et al, Nucl. Fusion **49** (2009) 104024
- [12] Nagatomo, H.; Johzaki, T.; Nakamura, T.; Sakagami, H.; Sunahara, A.; Mima, K., Simulation and design study of cryogenic cone shell target for fast ignition FIREX project, Phys. Plasmas, 2007, 14, 056303.
- [13] Johzaki, T., *et al.*, 2008 *Phys. Plasmas* **15** 062702.
- [14] A.Kemp and Y.Sentoku, Phy.Rev. E, 79, 066406 (2009)
- [15] S. Nakai et al IFSA2007 Proceeding Journal of Physics:Conference Series 112(2008)042070
- [16] K.Unlu, B.W.Wehring, J. Radioanalytical and Nucl. Chem. 217(1997)273
- [17] S.M. Whitney, et al. J.Radioanalytical Nucl. Chem.282(2009)173
- [18] R.Mateus, A.PJesus, B.Braizinh, J. Cruz, J.V. Pinto, J.P.Ribeiro, Nuclear instruments and methods B 190(2002)117-121
- [19] For an example, B.M.Hegelich, *Nature* 439, (2006) 441-444
- [20] UV Laser Ablations and Erosions to Investigate Fusion Reactor Surface Material Interactions, Hydrogen Storage Thin Layer Formations and the Related Subjects, K.Kasuya, K.Mima et al., 18th Gas flow and chemical lasers, and High power laser Symposium, Sofia, Bulgaria (2010) to be published.
- [21] ELM heat flux in the ITER divertor, A.Leonard et al., 1998 ICPP and 25th EPS Conf. On Contr. Nucl. Fusion and Plasma Physics, Prague, 29 June-3 July, ECA, vol. 22C, pp. 679-682, (1998).